J Wood Sci (2006) 52:51–57
DOI 10.1007/s10086-005-0714-y

ORIGINAL ARTICLE

Masahiro Noguchi · Shinjiro Takino · Kohei Komatsu

Development of wooden portal frame structures with improved columns

Received: December 17, 2004 / Accepted: February 22, 2005 / Published online: January 17, 2006

Abstract In Japan, the lifetime cycle of most housing lasts around 20–30 years. A governing factor in this respect is poor durability due to old-fashioned use of the house. As a solution of this problem, houses can be built with a skeleton structure that allows free partition of spaces by future owners. To develop the skeleton structure effectively, multistory frames with spans of 6 to 10 m are required. For this reason, attention has been focused on the behavior of multistory timber frame structures. In this article, two types of wooden portal frame structures are proposed. Both structures have improved vertical columns with short horizontal members glued in. The aim of this study was to investigate structurally effective solutions with these types of columns. The first type of the new structure changed the location of the moment-transmitting ductile connection with the improved columns. The second type of structure used an extended panel zone. Nine portal frame specimens were tested. The stiffness values were improved by around 1.7 and 3.5 times when compared with the control, and the strength was improved by around 1.25 and 1.45 times.

Key words Improved column · Timber · Portal frame · Multi-story · Semirigid

Introduction

In Japan, the lifetime cycle of most housing lasts around 20–30 years. This might be considered as a waste of resources and energy from a global environmental perspective. A governing factor in this respect is poor durability due to old-fashioned ideas about maintenance of the house. A way to solve this problem is to build houses with skeleton structures that allows free partitioning of spaces by future owners. To develop the skeleton structure effectively, multistory frames with spans of 6 to 10 m are required. For this reason, attention has been focused on multistory timber portal frame structures.

The approaches of much research in the past[1–8] focused on the improvement of structural performances by improving only the performance of the moment-transmitting connections. However, other parameters, such as the locations of the moment connections, members, and so on, are also important.

In this article, two types of timber portal frames are proposed. Both types have vertical columns with a short horizontal member added that is connected by adhesive as shown the shadow area in Fig. 1. These vertical members were defined as "improved columns." The aim of this article was to show the structural advantages of this type of improved column.

Material and methods

Concept

In portal frames of the type shown in Fig. 1, the behavior of the column–beam joints plays an important role in the structural performance. At this location, high peak bending moments usually appear. Timber joints should be able to transmit bending moments equal to the bending capacity of the timber members and have a semirigid moment rotation behavior. In most cases, high-strength joints behave rigidly having a brittle failure mode, while low-strength joints behave semirigidly. Semirigid behavior is beneficial for structural performance. Because the ideal connection does not yet exist, the idea was to create two different connections for the column–beam joint that satisfied both requirements. Besides the traditional column–beam joint, an additional semirigid joint was created at a location of low bending moments. For the first portal frames, the high capacity rigid joint at the column–beam intersection was maintained (type E), in Fig. 1.

M. Noguchi (✉) · S. Takino · K. Komatsu
Research Institute for Sustainable Humanosphere, Kyoto University, Gokasho, Uji 611-0011, Japan
Tel. +81-774-38-3670; Fax +81-774-38-3678
e-mail: noguchan@rish.kyoto-u.ac.jp

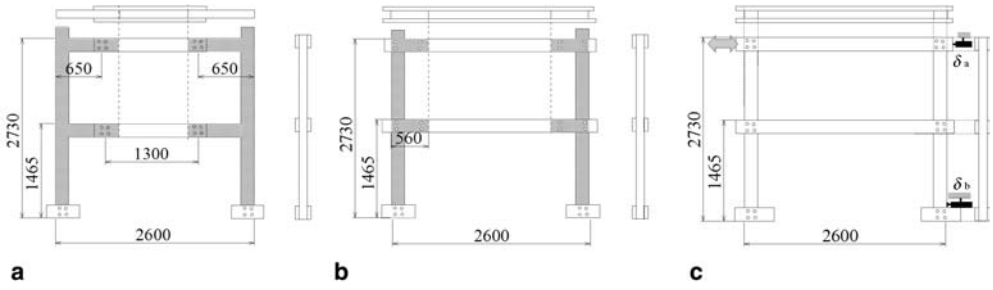

Fig. 1a–c. Diagrams of specimens. **a** Type E, **b** type S, **c** type C

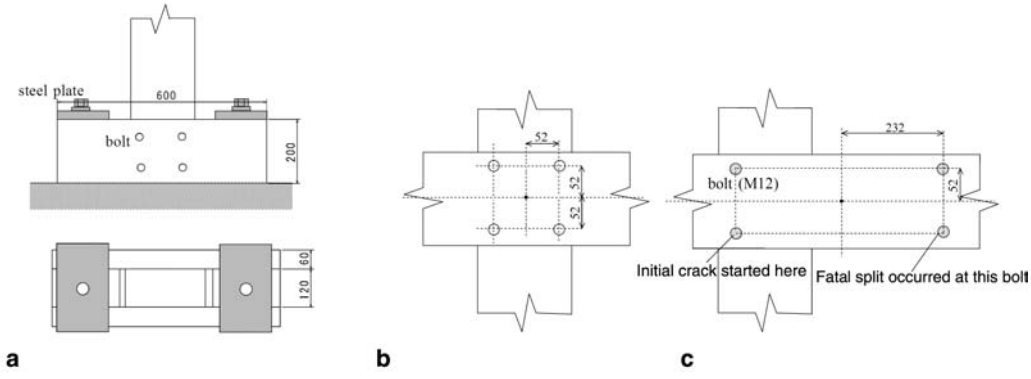

Fig. 2a–c. Joint detail. **a** Leg joint, **b** knee joint of type C, **c** knee joint of type S

For another portal frame, an additional semirigid joint is the structure where panel zones were extended (type S), in Fig 1. The panel zone, in this article, is defined as the overlapping area of the horizontal beam connected to the column and the horizontal member between the columns. The structural performances of moment-resisting joints is always limited by the area where column and beam overlap. If the height at the joint is increased, the strength capacity is larger. Maintaining the beam height while extending the overlap in the grain directions offers another opportunity to increase the moment capacity, see Fig. 2. The height is now governed by the minimal spacing between the bolts. This option also improves the connection stiffness. Finally, the portal frame with traditional bolted cross lapped joints is shown in Fig. 1 as the reference type (type C).

Test materials

In total, nine portal frames were built (three types × three replications). Each single column member was 3000 × 200 × 120 mm, double beam members were 3000 × 200 × 60 mm. All specimens were made of sugi (Japanese cedar, *Cryptomeria japonica*) glulam having JAS (Japanese Agricultural Standard) strength grade of E65 – f 220 [modulus of elasticity (MOE) 6500 MPa; modulus of rupture (MOR) 22 MPa]. The average timber moisture content was 11%. All specimens were two-story miniature semirigid frames. The column base connection is shown in Fig. 2a.

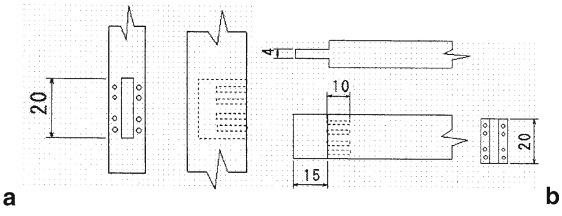

Fig. 3a,b. Construction of T-shaped member for the improved column. **a** Mortise and **b** tenon

Preparation of the improved columns

The joint between the column and the horizontal parts to form the "improved column" was made as follows. A rectangular hole was made in each column and eight holes were drilled as shown in Fig. 3. The dimensions of each rectangular hole were 200 × 30 mm, with a depth of 160 mm. The circular holes were 18 mm in diameter and 100 mm deep. The tenon member was made as shown in Fig. 3b. The central tenon had a width of 29.5 mm, a depth of 200 mm, and a tenon length of 155 mm. Similar to the mortise, each tenon had eight 18-mm diameter holes that were 100 mm deep and were drilled in the longitudinal direction.

The tenon and slender steel rods with diameter of 16 mm were driven into the rectangular hole and circular holes respectively, and they were fixed with epoxy resin adhesive using a sledgehammer. After the adhesive set, the F-shaped assembly was completed. We checked the adhesive injec-

Table 1. Load protocol

Cycle no.	Displacement angle R (rad)	Number of cycles
1	±1/240	3
2	±1/170	3
3	±1/120	3
4	±1/85	3
5	±1/60	3
6	±1/42.5	3
7	±1/30	3
Last	Until failure	

tion for enclosed air bubbles by observing the overflow of the adhesive from the holes. The insert length of the steel rod in each member was set to 100 mm. The time to cure was set to at least 2 weeks.

Assembly of portal frame specimens

The three portal frame types were assembled with single columns, double beams, and short bases joined with bolts as shown in Fig. 1. The clearance between bolts and predrilled holes was 1.5 mm, with hole diameters of 12 mm and bolt diameters of 10.5 mm. Figure 2b,c shows the bolt arrangement. The bolt arrangement of the type E frame was geometrically the same as that of type C.

Measurements and test procedure

The portal frame specimens were subjected to cyclic loading by applying a horizontal lateral force at the top of the specimens, as illustrated in Fig. 1c. Cyclic loading tests were carried out based on the protocol shown in Table 1. Story drift θ_{drift} was calculated by Eq. 1:

$$\theta_{\text{drift}} = \frac{\delta_{\text{a}} - \delta_{\text{b}}}{h} \tag{1}$$

where δ_{a} is the displacement of the roof beam (mm), δ_{b} is the displacement at the column base (mm), h is the distance between device for δ_{a} and that for δ_{b}.

Results and discussion

Failure mode

In type C specimens, failure did not occur until the end of the stroke length of the hydraulic actuator was reached. Bolted moment-transmitting joints yielded and then acted as plastic hinges, which resulted in a collapse mechanism. Similarly, type E specimens gave no failure up to the end of the stroke length. However, the collapse mechanism was different from type C specimens. Figure 4 shows the typical failure mode of type E specimens. As can be seen in Fig. 4, the failure did not occur at the intersection of the vertical and horizontal members, but at the location of the bolted moment-transmitting joints. This failure mode is mentioned in later discussion. In type S specimens, splitting failure occurred at the outer bolt hole in the moment joint as illustrated in Fig. 2c. The final and fatal failure that caused a considerable drop in load was due to splitting at the bolt hole and the timber beam (see Fig. 2c).

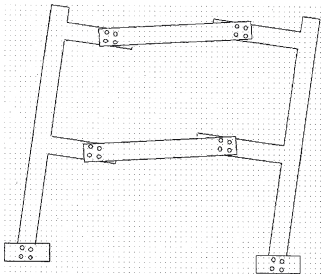

Fig. 4. Failure mode of type E specimens

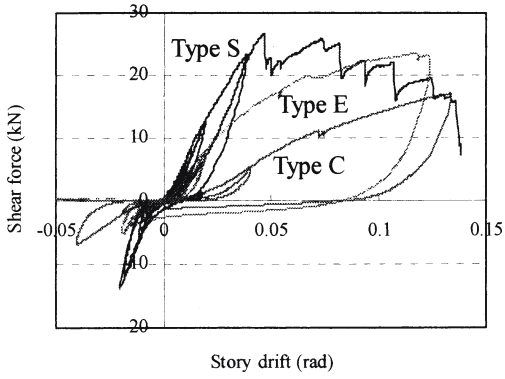

Fig. 5. Shear force–story drift relationship

Shear force – story drift curve

Typical shear force – story drift curves for the three different types of portal frame specimens are shown in Fig. 5. From Fig. 5, it is obvious that type E and S specimens have remarkable advantages in structural performance over the reference type, especially with regard to stiffness. Therefore, the portal frames proposed in this article obviously have higher potential for effective use in portal frames.

Stiffness

Table 2 shows the test results with respect to the initial stiffness determined by both visual readings (visual method) and the method proposed by the Japan Housing and Wood Technology Center (HOWTEC)[9] for the three different types of portal frame. The main difference between by the visual and HOWTEC methods is that the stiffness determined by the visual method did not consider the initial slip, while those by the HOWTEC method did. As can be seen in Table 2, the stiffness of type E and S

Table 2. Test results of stiffness

Specimen type	Specimen code	HOWTEC[a]	Stiffness visual	Calculated
Type E	E1	37204	43888	
	E2	30166	35520	43396
	E3	30845	40576	
	Average	32738	39995	
	S.D.	3882	4214	
	Ratio to type C	1.70	1.60	1.88
Type C	C1		23171	
	C2	20926	28142	23139
	C3	17553	23448	
	Average	19240	24920	
	S.D.	2385	2794	
	Ratio to type C	1.0	1.0	1.0
Type S	S1	64782	85218	
	S2	69172	89635	95224
	S3	76929	85255	
	Average	70294	86702	
	S.D.	6151	2540	
	Ratio to type C	3.65	3.48	4.12

[a] Method proposed by Japan Housing and Wood Technology Center[a]

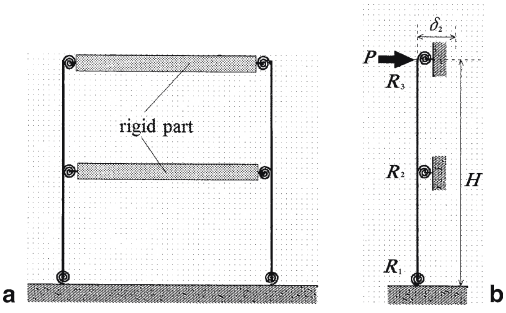

Fig. 6a,b. Model of vertical member. **a** Front view, **b** side view. H, Height of each story; R_1, rotational stiffness of leg joint; R_2, rotational stiffness of beam-joint resisting spring in first story; R_3, rotational stiffness of beam-joint resisting spring in second story; EI, bending stiffness of column; P, shear force

specimens are about 1.7 and 3.5 times larger than that of type C, respectively. The differences in stiffness between the HOWTEC method and the visual method were small.

In order to quantitatively explain the structural differences in performance of all three specimen types, a basic structural mechanics analysis was performed. First, considering the difference between type C and E specimens, only the horizontal members were different. In the discussion below, the story drift was examined with respect to the applied horizontal load. Without horizontal members, the columns deform as a cantilever beam. However, if the beam is connected to a column using a moment-transmitting connection, the column applies the reverse moment due to the resistance of the beam and the moment-transmitting joint at the nodes where the beam and column are connected. This transmitting moment plays a role in restraining the column deflection. When this transmitting moment is assumed as a rotational spring, type C and S specimens can be modelled

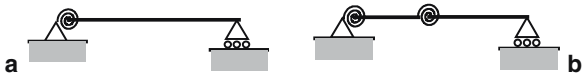

Fig. 7a,b. Model of horizontal member

as shown in Fig. 6a. Similarly, type E specimens can also be modelled as shown in Fig. 6a. In this article, this transmitting moment due to the resistance of the beam and the moment-transmitting joint is defined as a beam–joint rotation spring.

Focusing on the horizontal member and the moment-transmitting joint, it may be considered that the beam–joint rotation spring is composed of the moment-transmitting joint and the relationship between the rotation and the moment at point A. In general, the vertical displacement between the point at the center and the end of the beam does not occur when portal frame structures are modelled with horizontal load. Considering the above assumption and the symmetry condition, the beam–joint rotation spring of type S and C specimens can be modelled as shown in Fig. 7a. Similarly, type E specimens can also be modelled as shown in Fig. 7b, while vertical members having beam–joint rotation springs can be modelled as shown in Fig. 6.

The beam–joint rotation spring was modelled as a series of rotational springs of end connection and the slope angle at the end of the beam. Horizontal stiffness R was expressed using the rotational stiffness of the bolted moment joints R_j and the ratio of slope angle R_m.

$$R = \frac{R_j + R_m}{R_j \cdot R_m} \tag{2}$$

In type C specimens, classical beam theory can derived R_m as:

$$R_m = \frac{l}{3(EI)_l} \tag{3}$$

where l is half of span, and $(EI)_1$ is the bending stiffness of horizontal member.

For type E specimens, classical structural mechanics gives R as:

$$R = \frac{1}{\frac{\Psi_e}{3(EI)_1 l^2} + \frac{R_j \xi_e}{3(EI)_1 l^2} + \frac{\varphi_e}{Rl^2}} \quad (4)$$

where $\Psi_e = 3l^2t - t^3$, $\xi_e = -3tl^2 + l^3 - t^3 + 3t^2l$, $\varphi_e = t^2 - l^3$, and t is the distance between the joint and the center of the column.

The rotational stiffness of bolted cross lapped joints was calculated using Noguchi's model.[10] The Young's modulus of the material was taken as 6500 MPa, while the other properties were calculated by the regressions of Komatsu.[11] The stiffness ratio of type E and C specimens from Eq. 4 was 1.25. The observed stiffness ratio of type E and C specimens taken from the experiment was 1.6. This difference cannot be explained using only beam–joint rotation springs.

Next, using classical structural mechanics, the displacement at the top of the frame column (δ_2 in Fig. 6b) was derived as:

$$\delta_2 = \frac{H^3 P}{6EI} - \frac{H^2 P}{12EI} \cdot \frac{B}{A} \quad (5)$$

where

$$A = (R + R_2 - R_3)(EI)^2 + (R_2R_3 + R_1R_2)tEI + RR_2R_3t^2$$

and

$$B = -24(EI)^3 + (-12tR - 18tR_2)(EI)^2 + (-9Rt^2R_2 + 6t2R_2^2)EI + 3t^3RR_2^2$$

and H is the height of each story, R_1 is the rotational stiffness of the column base joint, R_2 is the rotational stiffness of the beam–joint rotation spring in the first story, R_3 is the rotational stiffness of the beam–joint rotation spring in the second story, EI is the bending stiffness of the column, and P is the shear force.

Table 2 shows the predicted values of stiffness of the structures based on Eq. 5, which is derived from basic structural analysis theory.

Next, the effects of the clearance between bolts and predrilled holes is discussed. In practice, hole clearances are always required to facilitate easy assembly of the structural components to erect the structures on site. However, the hole clearances introduces undesired initial lag in the behavior of the bolted cross lapped joints. Figure 8 shows the initial lag and shows the definition of the off-set value due to this phenomenon. As shown in Fig. 8, the ratio of the average off-set value of type E and S specimens with respect to type C were a half and a quarter, respectively. Figure 8b shows the distributions of the off-set values of the three types. From Fig. 8 it is noted that the off-set value for both type E and S specimens were much smaller than of type C.

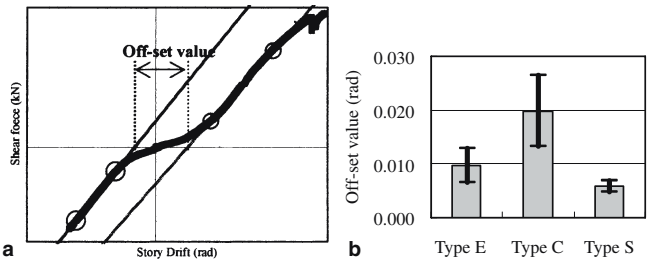

Fig. 8a,b. Definition (a) and values (b) of off-set

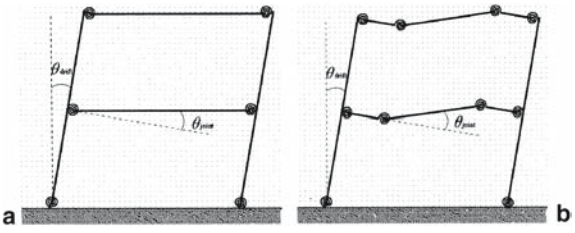

Fig. 9a,b. Collapse mechanism for **a** type C specimens and **b** type E specimens

The reason for this difference might be that in type E specimens, it was thought that the rotational angle was not the same as the story drift angle. However, in the type S specimens, the distance between the center of rotation and each bolt was much larger than that in type C specimens (type C 73.5 mm, type S 237 mm). As the initial rotational slip is roughly inversely proportional to the distance of the rotation center of joint, the off-set of type S specimens was around 25% of that of type C specimens.

Generally speaking, secondary stresses occur in statically indeterminate structures, when the dimensions of the members change as a result of moisture changes. In the case of the portal frame structure with bolted knee joints having some hole clearances, i.e., the structure proposed in this article, these secondary stresses probably do not appear. There is a lack of information about this issue in timber engineering. Therefore, it is thought the hole clearance has some benefit in counteracting secondary stresses.

Strength and ductility

Average yield, ultimate and maximum strengths, and standard deviations for the three different types of portal frames are shown in Table 3. As can be seen in Table 3, the strength ratios of type E and S specimens are around 1.25 and 1.45 times larger than that of type C specimens, respectively. The differences in strength ratio among the specimens of one type was small. Because the failure mechanism of both type E and C specimens was caused by failure of the bolted cross lapped joints the differences in yield mechanism were explained with the classic yield failure model, as shown in Fig. 9. With type S specimens failing at the T-shaped member in a brittle manner, the same failure mecha-

Table 3. Test results for strength of ductility

Specimen type	Specimen code	Maximam load P_{max} (kN)	Yield load P_v (kN)	Ultimate load P_u (kN)	Energy absorption (kNm)	μ
Type E	E1	23.36	13.27	20.91	5.36	2.19
	E2	20.76	11.81	19.23	5.92	2.29
	E3	27.78	12.83	23.38	5.38	1.62
	Average	23.97	12.64	21.17	5.55	2.03
	S.D.	3.55	0.75	2.09	0.31	0.36
	Ratio to type C	1.48	1.33	1.53	1.43	1.26
Type C	C1	10.23	7.60	9.25	3.53	
	C2	19.13	9.40	15.81	3.82	1.68
	C3	19.15	11.49	16.51	4.34	1.53
	Average	16.17	9.50	13.86	3.89	1.61
	S.D.	0.01	1.48	0.49	0.41	0.11
	Ratio to type C	1.00	1.00	1.00	1.00	1.00
Type S	S1	26.61	14.20	23.14	6.47	3.00
	S2	24.02	15.86	21.50	2.18	1.60
	S3	30.48	16.94	26.95	8.56	3.86
	Average	27.03	15.66	23.86	5.74	2.82
	S.D.	3.26	1.38	2.79	3.25	1.14
	Ratio to type C	1.67	1.65	1.72	1.47	1.75

nism could not be applied. The external work W can be expressed by the following equation.

$$W = P\theta_{\text{drift}} \tag{6}$$

where P is shear force.

In the case of type C specimens, internal energy U was expressed as:

$$U = 6\sum M\theta_{\text{drift}} \tag{7}$$

where M is the ultimate moment at the bolted joint in type E and C specimens.

From Eqs. 6 and 7, the shear force was obtained as:

$$P = 6\sum M \tag{8}$$

In the case of type E specimens, internal energy was expressed as:

$$U = 4\sum M\theta_{\text{joint}} + 2\sum M\theta_{\text{drift}} \tag{9}$$

From Fig. 9, the ratio of θ_{joint} to θ_{drift} can be expressed by the following equation.

$$\theta_{\text{joint}} = \frac{l}{t}\theta_{\text{drift}} \tag{10}$$

From Eqs. 6, 9, and 10, shear force was obtained as:

$$P = \left(4\frac{l}{t} + 2\right)\sum M \tag{11}$$

Using Eqs. 8 and 11, the ultimate strength ratio of type E specimens to type C specimens can be derived as:

$$r_{\text{ec}} = \frac{\left(\frac{2l}{l_a} + 1\right)}{3} \tag{12}$$

In the case of type E specimens, $l_a = \frac{1}{2}l$, and $r_{\text{ec}} = 1.66$.

The observed average strength ratio of type E and C specimens was 1.53, which is somewhat lower than 1.66. It is thought that this difference can be ignored because the elastic deformations (energies) of the members in this model were not taken into account by this failure mechanism. For this reason it is assumed that this model takes into account the most important parameters. This implies that for type E specimens the ultimate strength is linked to properties of the joint and the story drift. Table 3 also shows the energy absorption and ductility ratio for the three different types of portal frames.

As Table 3 shows, the average energy absorptions of type S and type E specimens were 1.47 and 1.43 times larger than that of type C specimens, respectively. The average ductility ratios of type S and type E specimens were also 1.47 and 1.43 times larger than that of type C specimens, respectively. The two semirigid frames proposed have advantages in energy absorption.

Conclusions

One traditional and two modified portal frame structures were compared in this study. The modified structures have improved columns. Added to the first modified frame was an extra joint located in the low-stressed part with ductile behavior. In the second type, the joint area or panel zone was extended. With respect to the traditional frame, the stiffness of the modified frames improved by around 1.7 and 3.5 times, while the strength increased by around 1.25 and 1.45 times, respectively. Moreover, the average energy absorption of type S and type E specimens were 1.47 and 1.43

times larger than that of type C specimens, respectively. Therefore, the portal frame structures with improved columns have structural advantages, especially with regard to stiffness.

References

1. Leijten AJM (1998) Reinforced joints with expanded tube fasteners. In: Densified veneer wood reinforced timber joints with expanded tube fasteners. Delft University Press, Delft, pp 57–96
2. Leijten AJM (1988) Steel reinforced joints with dowels and bolts. In: Proceedings of International Conference on Timber Engineering, Washington, vol 2, pp 475–488
3. Haller P, Chen CJ, Natterer J (1996) Experimental study on glass fibre reinforced and densified timber. In: Proceedings of International Wood Engineering Conference, New Orleans, USA, vol 1, pp 308–314
4. Haller P (ed) (1999) Final report of COST C1 Working Group Timber Joints – Semi-rigid timber joints, structural behaviour, modelling and new technologies. Univ. Dresden, Germany
5. Leichti RJ, Tjahyadi A, Bienhaus A, Gupta R, Miller T, Duff S (2002) Design and behaviour of frictio dampers for two-dimensional braced and moment-resisting timber frames. In: Proceedings of World Conference on Timber Engineering, Shah Alam, Malaysia, vol 2, pp 267–274
6. Rodd PD (1996) Resin injected dowels in moment transmitting joints. In: Proceedings of International Wood Engineering Conference, New Orleans, USA, pp 169–176
7. Ohashi Y, Sakamoto I (1989) Study on laminated timber moment resisting joint. In: Proceedings of the Second Pacific Timber Engineering Conference, Auckland, New Zealand, vol 2, pp 37–42
8. Komatsu K, Karube M, Harada M, Fukuda I, Hara Y, Kaihara H (1996) Strength and ductility of glulam portal frame designed by considering yield of fasteners in part. In: Proceedings of International Wood Engineering Conference, New Orleans, USA, pp 523–530
9. Building Center of Japan (2002) The building letter. 443:27–32
10. Noguchi M, Komatsu K (2003) A new proposal for estimating method of stiffness and strength in the bolted timber-to-timber joints and its verification by experiments (II): bolted cross lapped beam to column joints. J Wood Sci 50:391–399
11. Architectural Institute of Japan (AIJ) (1995) Moment resisting joints (in Japanese). In: Structural design note for timber structures. Maruzen, Tokyo, pp 184–221